Available online at www.sciencedirect.com
ScienceDirect
Cement and Concrete Research 37 (2007) 351–359
Cement and Concrete Research

Toolbox for 3D imaging and modeling of porous media: Relationship with transport properties

P. Levitz

Laboratoire de Physique de la Matière condensée, Ecole Polytechnique-CNRS, 91128, Palaiseau, France

Received 5 October 2005; accepted 16 August 2006

Abstract

Porous media can be considered as interfacial systems where an internal surface partitions and fills the space in a complex way. Meaningful structural features appear on a length-scale where physical chemistry plays a central role either to impose a specific organisation on the material or to strongly modify the dynamics and the thermodynamics of the embedded fluids. A key issue is to understand how the geometrical and interfacial confinement affects numerous phenomena such as molecular diffusion, excitation relaxation, reaction kinetics, phase transitions, adsorption and capillary condensation. We will first review some experimental techniques able to image the 3D structure of disordered porous media. In the second part, we will analyse the geometrical and particularly some topological properties of a disordered porous material. We will discuss the interest and the limits of several strategies for obtaining 3D representations of various pore networks starting from an incomplete set of morphological characterisations. Finally, connection between geometry and diffusive transport will be presented, with emphasis on the application of pulsed gradient spin echo NMR technique as a tool for a multiscale analysis of transport in a confining geometry.

Keywords: Porous media; Morphology; Topology; 3D imaging; Small angle scattering; Diffusive transport; Pulse gradient spin echo NMR

1. Introduction

A mesoscopic divided matter and/or material (MDM) is an interfacial system where an internal surface partitions and fills the space in a complex way. MDM meaningful structural features appear on a length where physical chemistry plays a central role to impose a structure and a specific arrangement of constituent parts of the material (texture). The mesoscopic scale often coincides with the colloidal scale (submillimetric and lower). Pastes, slurries, cements, concretes, cokes, soil, catalysts, wood, paper coating, organised molecular systems, and ceramics are a few examples of MDM. Many of these materials can also be considered as disordered porous materials.

Looking at the interfacial properties of these media, especially the role of curvature, we can propose a preliminary textural classification. First, some materials are made of well-defined particles. In other words, we are dealing with a granular medium. In the case of clay pastes, each particle appears as a flat membrane at the atomic scale. These membranes can be strongly crumpled as encountered for a coke microtexture. By elimination of interfacial boundaries we get a collection of distinctive individual particles such as spheres, ellipsoids, needles, or globular particles. Finally, the internal interface can be considered as a whole, multiconnected in space without borders which is archetypal of biphasic disordered porous media, exhibiting a more or less complex topology. Triply periodic minimal surfaces [1] encountered in oil–water, lipid, block copolymer and other amphiphilic systems, and templated nanostructured solid surfaces such as MCM48 [2], all belong to this class of MDM.

The degree of disorder is another way to classify MDM textures. A large class of MDM is relatively homogeneous with a defined disorder length-scale. It is then easy to find a representative elementary volume (REV), such that averages of physical properties are possible and meaningful. In the following, such matrix will be called “weakly disordered textures”. On the other hand, several materials exhibit strong disorder and heterogeneity at different length-scales. In this case a REV cannot be defined and any averaging is length-scale sensitive. The fractal geometric [3,4] description provides a simple way to go from one to another length-scale. The associated geometrical

E-mail address: levitz@pmc.polytechnique.fr.

0008-8846/$ - see front matter © 2006 Published by Elsevier Ltd.
doi:10.1016/j.cemconres.2006.08.004

transformation is based on statistical length-scale invariance. A fractal object keeps the same statistical morphology on a magnification or a change of scale. Two interesting properties can be mentioned at this level. First, let us try to tile the fractal matrix with a collection of yardsticks having a typical size ε. The total number of yardsticks needed to cover the all object is proportional to ε^{-df}. Here d_f is the fractal dimension ranging between 0 and 3. Secondly, for a self-similar structure, the mass contained inside a box of size L evolves as L^{df}. Fractal geometry can be applied in numerous other cases. However, some hierarchical textures having specific organisation at different length-scales are still difficult to describe as a "whole".

A key issue is to understand how the geometrical and interfacial confinement affects numerous phenomena such as molecular diffusion, excitation relaxation, reaction kinetics, phase transitions, adsorption and capillary condensation [5,6]. This raises the challenge of describing the geometry of the pore network. Three levels of analysis are encountered in the literature. At the first level, apparently the most simple, the aim is to obtain a few numbers, which characterise the global properties of the porous material. One can first ask how much space the pore network occupies. One can introduce the porosity, ϕ, defined as the ratio of void (or pore) volume over total sample volume. A subtler question deals with the overall amount of interface per unit of volume (S_v). However, ϕ and S_v do not provide any clear information about the morphology of the pore network. One has to reach a second level of characterisation where questions are raised about average pore size mean curvature, pore shape, surface roughness, structural correlation between points belonging to the solid, the interface or the pore network. Finally, the last level concerns a topological analysis of the matrix [7,8], which is closely related to the long-range connectivity or percolation of pore network (Gauss curvature of the interface $\langle K \rangle$, deformation retract, genus of the interface). Several interesting properties should be analysed at this level such as the number of available paths linking two distinct points of the pore network, the metric distance between two points compared to their shortest (geodesic) distance and the important role of pore throats. It is clear that several terms are ill defined or ambiguous. This is for example the case for the average pore shape of a disordered pore network. It becomes evident that porous media *must be characterised in statistical terms*. One important goal is to handle correctly the pore structure at different length-scales in relation to the thermodynamics and molecular dynamics inside these confined and often disordered geometries.

In this paper, we first introduce the challenging problem of obtaining a reliable description of the MDM texture. In the second part, we discuss temporal and spatial properties of molecular confined dynamics inside porous materials and their potential connections with experiments such as pulse field gradients NMR.

2. Experimental tools

2.1. Some imaging techniques

Experimental imaging techniques play an important role in understanding the structure of mesoscopic disordered media and more particularly the geometrical organisation of porous materials. It is relatively "easy" to provide 2D images of the material at high resolution, using either transmission electron microscopy (TEM, resolution up to some Å) or scanning electron microscopy (SEM). One tedious way to get a 3D reconstruction is to perform serial sections as close as possible to each other (that is the major limiting factor) and piling them up. Such a protocol was used to analyse soil [9] (see Fig. 1). Generally, this difficult and tedious work cannot be performed at the same resolution (as high as possible) in the three spatial directions. However, a novel serial sectioning procedure for 3D analysis using a dual-beam FIB (focused ion beam) was recently proposed [10]. The acquired stack of images can be transformed directly into 3D data volume with a voxel resolution of 15 nm. Several other techniques to get 3D images of various materials are available. Among them, we can mention Magnetic Resonance Imaging (see Fig. 2 and [11,12]) or X-ray microtomography (see Fig. 3) which are generally non-invasive but with typical resolution not lower than 0.1 μm. Another interesting approach is the TEM tomography [13] already used to image biological materials at very high resolution. In the near future, optics of coherent X-rays will certainly provide new 3D imaging methods at higher resolution.

2.2. Structural correlation and small angle scattering techniques

Another alternative to probe the MDM morphology is to look at structural correlations [14,16]. The goal is to correlate the structural state (i.e. with reference to the solid matrix or to the internal interface) of two distinct points separated by a distance r. These structural correlations quantify how the 'memory' of an initial state is progressively lost when a point is moved away. Two-point correlation functions such as the bulk, the surface autocorrelation or the pore-surface correlation functions can be defined. They play a central role in different processes involving energy, excitation or molecular transport. Moreover, as shown in the seminal work of Doi [15,16], these three correlation functions are directly involved in an upper bound limit of the permeability. Clearly a statistical geometrical analysis of these two-point correlation functions is required. Debye et al. [17] performed one

Fig. 1. 3D reconstruction of the soil core by serial sectioning. The pixel resolution is 100 μm (adapted from [9,10]). The region of interest is 1 mm in dimension.

of the first contributions in this direction. Interestingly, 3D structural correlations can be experimentally probed, using small angle X-ray or neutron scattering (SAXS, SANS) [18–21]. Such methods are generally non-invasive. It is well known that the density fluctuations are the main origin of the scattering. In the case of a biphasic matrix, these fluctuations are localised just at the sharp interface which partitions the system. The small angle scattering, considered as a purely interfacial phenomena, is then strongly dependent on the geometrical properties of this oriented interface. This statement can be qualitatively understood if we consider a disordered porous medium as being completely defined either by its mass distribution or by the oriented interface separating the pore network and the solid matrix. Properties of the second derivative of the mass autocorrelation function quantitatively define the level of connection between small angle scattering and the statistical properties of the interface [20–22]. According to classical theory, the small angle scattering $I(\mathbf{q})$ is related to the 3D Fourier transform of the fluctuation autocorrelation function $\eta^2(\mathbf{r})$. $\eta^2(\mathbf{r})$ correlates the structural state (i.e. with reference to the solid matrix or to the internal interface) of two distinct points separated by a distance r. The structural state at point $\mathbf{r}$ is defined as the difference between the mass distribution $\rho(\mathbf{r})$ and the volume average of $\rho(\mathbf{r})$, noted $\langle\rho\rangle$. It involves a density contrast which in fact determines the scattering properties of a porous medium. $\eta^2(\mathbf{r})$ is written as:

$$\eta^2(\mathbf{r}) = \frac{1}{V}\int \mathrm{d}\mathbf{r}_0(\rho(\mathbf{r}_0)-\langle\rho\rangle)(\rho(\mathbf{r}_0+\mathbf{r})-\langle\rho\rangle) \quad (1)$$

Following Witten's argument, one can evaluate the primary evolution of $I(q)$ if one looks at the density fluctuations inside an average sphere of size $1/q$, located in such a way that a part of the interface belongs to the sphere. The rule of thumb is written as

$$I(q)\alpha \mathrm{Nb}(1/q)\cdot[\mathrm{Mb}(1/q)]^2 \quad (2)$$

where $\mathrm{Nb}(1/q)$ is the total number of spheres tiling the structure. $\mathrm{Mb}(1/q)$ is the average mass per sphere. Let us first consider a collection of independent thin discotic particles of radius R and thickness e. For $e<1/q<R$, one gets $\mathrm{Nb}(1/q)\alpha q^2$ and $\mathrm{Mb}(1/q)\alpha 1/q^2$. The main term for $I(q)$ is therefore dependent on $1/q^2$. In the same q range and for rod-shaped particles, one can check that $I(q)\alpha 1/q$. Such results provide direct information on particle shape. They can be extended to the case of length-scale invariant structures.

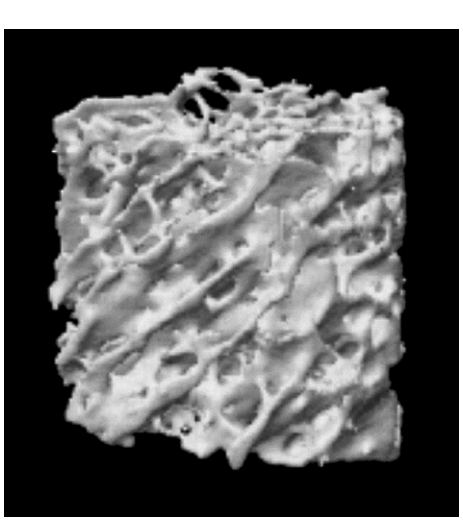

Fig. 2. Three-dimensional visualisation of a trabecular bone. The binary image is obtained by Magnetic Resonance Imaging [11,12]. The voxel resolution is 40 μm.

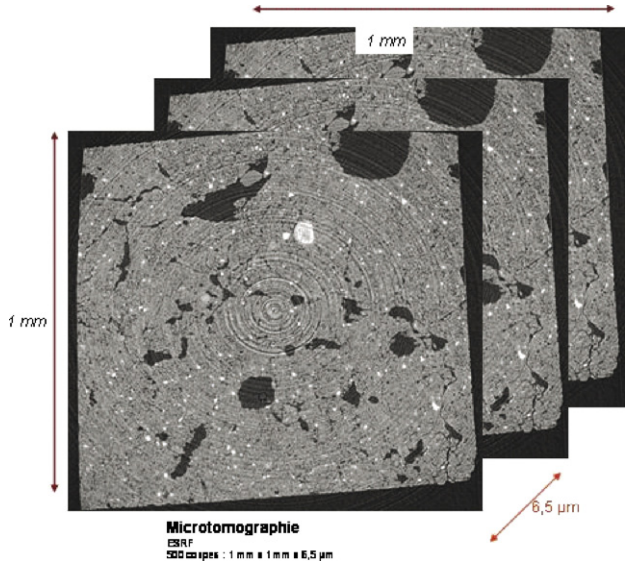

Fig. 3. X-ray microtomography of a soil pore network (P. Levitz-CNRS, I. Cousin-INRA, ESFR-Grenoble). The lateral voxel resolution is 1 μm.

For mass fractal, the number of yardsticks, of size $1/q$, tiling the matrix runs as $1/(1/q)^{d\mathrm{m}}$ where d_m is the mass fractal dimension. The mass of a sphere of radius $1/q$ is $\mathrm{Mb}(1/q)\alpha(1/q)^{d\mathrm{m}}$. One then gets the well known result $I(q)\alpha 1/q^{d\mathrm{m}}$.

Let us finally consider the case of a surface fractal structure. As above, $\mathrm{Nb}(q)\alpha q^{ds}$ where d_s is the surface fractal dimension. However, the interface is the only length-scale invariant feature and $\mathrm{Mb}(q)\alpha(1/q)^3$. Now $I(q)$ evolves as $1/q^{6-\mathrm{ds}}$ [23]. For a smooth interface ($d_\mathrm{s}=2$), one obtains the well-known Porod regime, which is dependent on S_v/q^4. In mesoscopic porous media, the Porod regime is generally observed in the high q range, above 0.1 $\mathrm{Å}^{-1}$. In this q regime, negative departure from the Porod law must be analysed with caution. As shown elsewhere [24], atomic roughness can induce such negative departure, which can be roughly analysed in terms of a self-affine surface with a low upper cut-off.

In conclusion, small angle scattering is a direct experimental way to probe correlation and interfacial properties of porous materials, providing direct textural information on both weak and strong disordered textures.

3. Basic toolbox to capture forms and patterns

3.1. Morphology

Since our aim is to discuss and to analyse forms, shapes and patterns, it is useful to recall some morphological tools. At present, it is difficult to provide three-dimensional (3D) representations of many MDM using conventional or more

sophisticated 3D imaging techniques. It is more convenient to work on 2D sections of the material. Among all possible metric parameters, it is interesting to identify those global parameters, which can be estimated in either 2D or 3D. This is the aim of stereology [8]. These parameters have to satisfy a number of criteria, the so-called Hadwiger conditions [8]: (1) they have to be invariant by translation or by rotation of the material; (2) they have to satisfy the homogeneity conditions; (3) they have to be continuous functions; (4) they have to satisfy the additivity conditions. Under such constraints, four functionals (also called Minkowski invariants) can be defined: the porosity, the specific surface area, the integral of mean curvature and the integral of Gaussian curvature. The first three can be measured on 2D sections while the last one, related to the topology of the pore network, can only be estimated on 3D representations. As shown in Fig. 4, two principal radii of curvature R_1 and R_2, the maximum and the minimum respectively, can be defined at any point s on the interface. If $k_1=1/R_1$ and $k_2=1/R_2$ are the two principal curvature at point s, the mean curvature is defined as

$$H(s) = (k_1 + k_2)/2 \tag{3}$$

whereas the Gaussian curvature is

$$K(s) = k_1 \cdot k_2 \tag{4}$$

The integral of the mean curvature per unit volume, M_v, is calculated by integration of the mean curvature over all the interface contained in a volume V. The integral of the mean curvature may also be determined on a 2D section of the porous material [8].

Chord distribution functions [20–22,25] provide a way to get a more complete stereological analysis of the MDM. These functions can be computed either in 2D or 3D assuming some general conditions similar to Hadwiger's. Their determination helps us to clarify some questions about average pore size, mean curvature, pore shape, surface roughness and structural correlation between points belonging to the solid, the interface or the pore network.

A chord is a segment belonging either to the pore network (p) or to the solid matrix (m) and having its two extremities on the interface. There are several ways to define chord length distribution functions depending of the chosen angular average. In the following, we use the classification introduced by Colemam [25] and discuss mainly the μ-chords properties. As shown in Fig. 5, μ-chords are obtained by tracing random and homogeneously distributed straight lines (rays) through a section or a 3D structure. The chord length distribution function gives the probability of having a chord length between r and $r+dr$ belonging either to the pore network ($f_p(r)$) or to the solid matrix ($f_m(r)$).

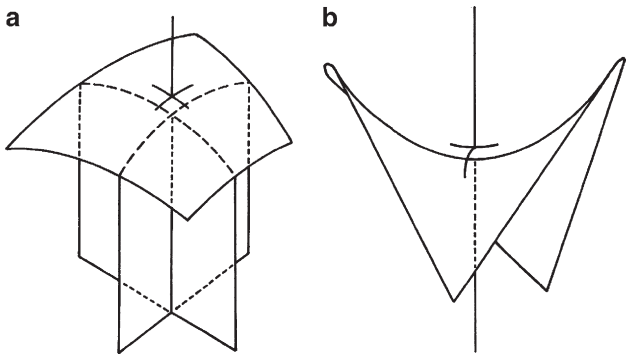

Fig. 4. (a) Minimum and maximum curvature radius of a surface. The surface has positive mean and Gaussian curvatures. (b) Example of a saddle point with a negative Gaussian curvature.

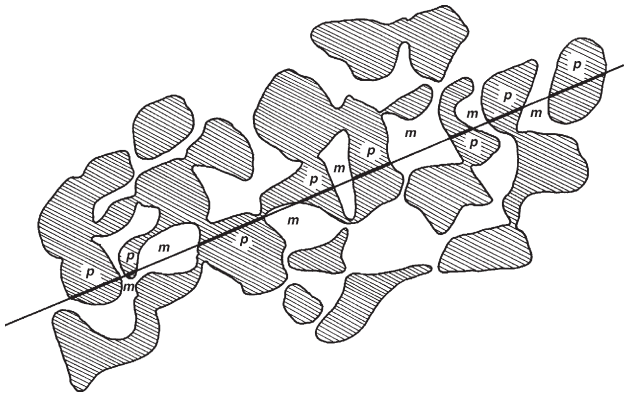

Fig. 5. μ-Chords through a porous media (adapted from Ref. [20]).

The μ-chord distribution functions can either be computed inside a 3D structure or through a random section of the pore network. In both cases, the final results will be similar, assuming some general properties such as statistical isotropy. If $\langle l_p\rangle$ and $\langle l_m\rangle$ are the average chord length in the pore network and in the solid matrix respectively, then

$$\phi = \langle l_p\rangle/(\langle l_p\rangle + \langle l_m\rangle) \tag{5}$$

and

$$S_v = 4\phi/\langle l_p\rangle = 4(1-\phi)/\langle l_m\rangle \tag{6}$$

The two first Minkowski invariants, namely ϕ and S_v, are directly related to the first moments of $f_p(r)$ and $f_m(r)$.

Chord distribution functions are sensitive to the type of structural disorder. This point is discussed elsewhere [21] and allows us to consider μ-chord distribution functions as fingerprints of the local and semi-local morphology of the pore network. As examples, we see in Fig. 6 three different types of porous media. The first material is a section of dolomite (Fig. 6a, b). Above a few pixels, the pore and solid chord distribution functions evolve according to a negative exponential tail.

$$\begin{aligned} f_p(r) &\alpha \exp(-r/\lambda_1) \\ f_m(r) &\alpha \exp(-r/\lambda_2) \end{aligned} \tag{7}$$

where λ_1 and λ_2 are the persistence lengths for the porous phase and the solid matrix respectively. λ_1 can be considered as the mean size of the pore (in white). This material is a good example of a long range Debye random medium [17,21].

A granular material composed of smooth convex particles (see Fig. 6c, d) provides another interesting example. The pore

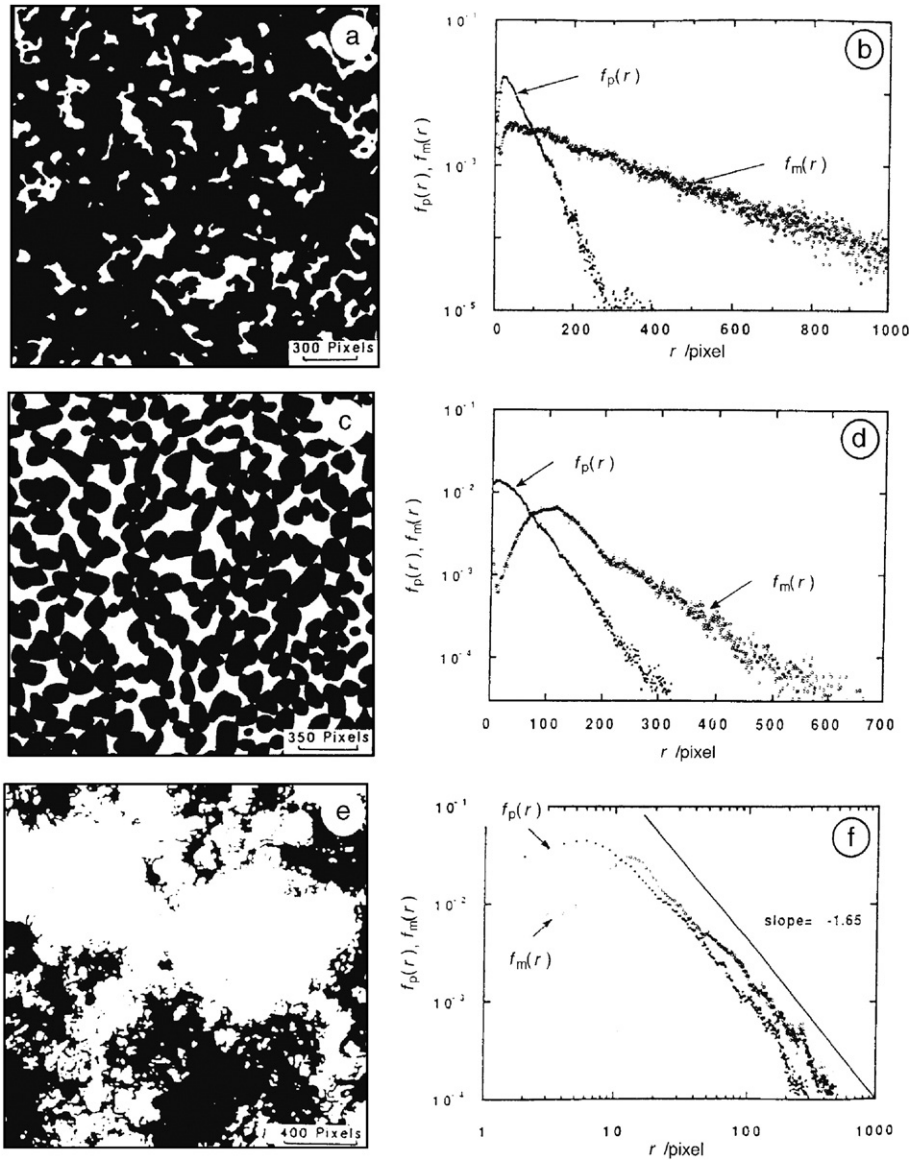

Fig. 6. Digitised images of thin sections of various porous media and corresponding pore and solid chord distribution functions (pore in white and solid in black): dolomite (a), granular medium (b) and cement paste (c) (adapted from Ref. [21]).

chord distribution shows a linear increase at small distances (smooth interface) followed by an exponential decay at larger distances. Again, a persistence length can be defined and gives a good estimation of the average pore size. The solid chord distribution function exhibits a peak followed by an exponential tail. This curve provides direct information about the average shape (spheroid, elongated, rod-like, etc.) of convex particles and particularly about their mean diameter.

Let us now consider complex porous materials with length-scale invariance. For a biphasic medium having a fractal distribution of mass, as encountered for example in diffusion-limited aggregates or cluster-cluster structures, we get [21]:

$$f_p(r)\alpha 1/r^{d_m-1} \tag{8}$$

where d_m is the mass fractal dimension.

Finally, for a porous medium with a fractal surface (see Fig. 6e, f), the pore and the solid chord distribution functions scale in a similar way as [21]:

$$f_p(r)\alpha 1/r^{d_s-1} \tag{9}$$

$$f_m(r)\alpha 1/r^{d_s-1} \tag{10}$$

where d_s is the fractal dimension of the internal interface.

These few examples show that the morphological properties of a porous medium (at the scale of the pore element) can be demonstrated by chord distribution functions.

3.2. Topology and curvature

An important question concerns the connectivity of the pore network (or the solid matrix) at different length-scales. A

geometrical set X is interconnected when every pair of points belonging to X may be joined by a curve included in X. Clearly, the MDM connectivity is an important characteristic for transport properties such as molecular diffusion or fluid permeability. As already stated, the pore network is essentially defined by its internal interface; the topology, mainly the connectivity, is related to the genus G of this interface [7]. The genus of a surface is the maximum number of ways a surface may be cut by closed loops without losing its initial connectivity. $G=0$ for a sphere and $G=1$ for a torus. The genus is not additive and it is necessary to introduce another topological parameter, the Euler Poincaré constant N_3 of the pore network [7,8]:

$$N_3 = \sum_{i=1}^{i_{\max}} (1-G_i) \tag{11}$$

where $i_{\max}$ is the number of disconnected surfaces delimiting the pore network. N_3 is additive and is directly related to global curvature properties of the internal interface by:

$$N_3(X) = \frac{1}{4\pi}\int_{\partial X} k_1 k_2 \mathrm{d}S \tag{12}$$

where the surface integral is performed in the surface delimiting the set X. In the case of a collection of disconnected particles, N_3 is exactly the number of objects. For a pore network delimited by a unique multiconnected interface having a genus G, N_3 is equal to $1-G$.

A powerful tool to describe the architecture of porous media is the linear graph of retraction [7,11,26]. This graph is obtained by progressively narrowing the pore space starting from the internal surface. This 'thinning skeletizing' must satisfy both topological (invariance of the three first Betty numbers [11,26]) and geometrical constraints in order to fit as exactly as possible the "skeleton graph". A difficult step is to reduce the numerical skeleton in terms of a simple graph made of vertices connected by edges and having the same topological properties. A numerical scheme was recently proposed to provide a numerical solution to this delicate problem [11]. As shown in Fig. 7, we end up with a simple 3D map of the pore network. The Euler Poincaré constant can be rewritten as

$$N_3 = \alpha_0 - \alpha_1 = \alpha_0(1-N_c/2) \tag{13}$$

where α_0 and α_1 are the number of vertices and edges respectively. N_c is the average number of nearest neighbor vertices. Theoretical and experimental works on fluid flow indicate that this statistical coordination number is one of the few important parameters for that application.

The knowledge of the pore network and the linear graph of retraction opens the possibility to define and to extract "elementary pores" and to analyse their statistical morphology in relation with transport and mechanical properties.

3.3. Modeling of pore network

A challenging question is to find a way, if it exists, to provide a realistic 3D configuration of a pore network at the right length-scale. When direct 3D images are not available, two possible strategies are possible. The first way is to simulate or to mimic physical and chemical processes directly acting during elaboration of the medium. The former mimetic simulation techniques have several advantages. Mainly, they provide an understanding of the physics and the chemistry behind the formation of a porous material. However, such approach has to be done on a case-by-case basis. Moreover, the finite size of simulated systems is actually a real technical difficulty especially when the simulation

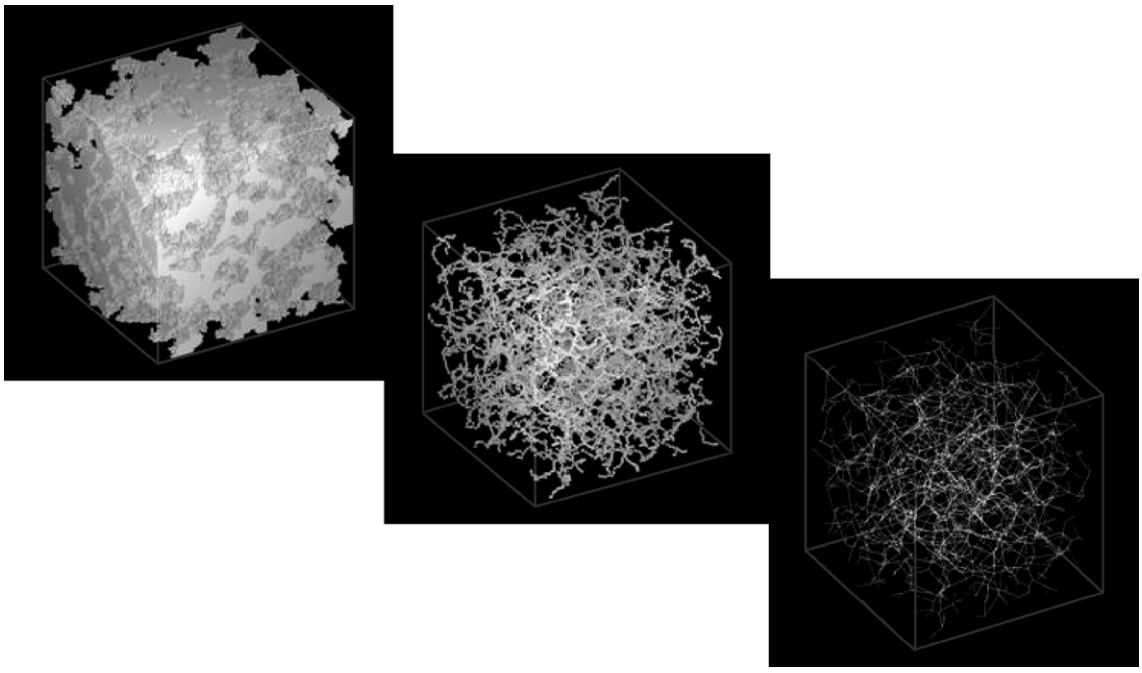

Fig. 7. Linear graph of retraction of a porous membrane of filtration.

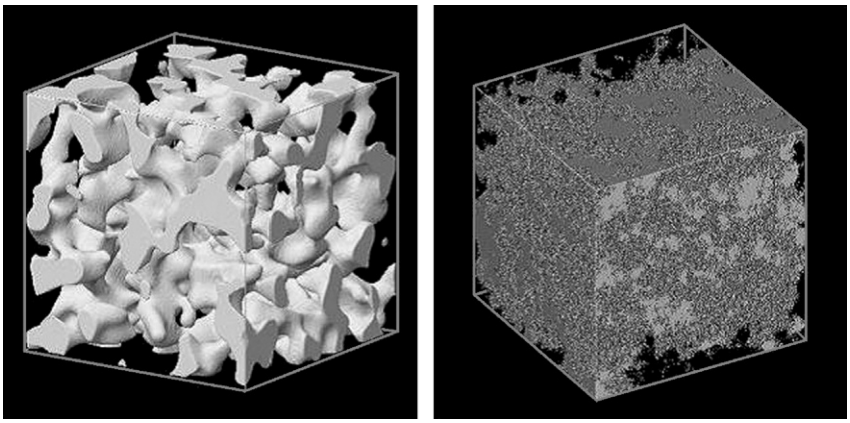

Fig. 8. On the left, 3D off-lattice reconstruction of a Vycor-like porous glass [29–31]. The pore network is in white. The edge of the cube is 100 nm. On the right, reconstruction of a cement paste [29–31].

is performed at the atomic scale. It is generally difficult to sample long range connectivity and large representative elementary volumes. An alternative strategy to modeling the material is to perform a reconstruction of the material from limited but relatively accurate structural information about the original system, mainly 2D images of a random section and small angle scattering of the matrix. This is an inverse problem that has no general and exact solution. However, it is important to evaluate available methods able to solve such a problem with a good level of approximation. In the following, we discuss stochastic reconstructions using either correlated Gaussian fields or simulated annealing.

3.3.1. 3D reconstruction using correlated Gaussian fields

Starting from the knowledge of bulk autocorrelation function of the matrix, it is possible to rebuild a 3D pore network having the same characteristics (meaning having similar specific surface area, pore volume and bulk–bulk correlation function). Such reconstruction is based on the use of correlated Gaussian fields [27–31]. Two examples are shown in Fig. 8 related to a realistic 3D model of the Vycor porous glass and a possible reconstruction of a cement paste. Critical evaluation of these reconstructions and comparison with experiments are discussed in [30,31].

3.3.2. 3D reconstruction using simulated annealing

The former strategy based on Gaussian random fields gives the successful reconstructions of many classes of nonparticulate composite materials. However, with several systems such as granular materials, additional morphological information is required. It is then necessary to go beyond the two-point correlation function and add other types of correlation functions in order to get a more constrained reconstruction procedure. Several authors have recently proposed another stochastic reconstruction technique based on a simulated annealing method [32]. Using either a 2D section of the material or information from small angle scattering, it is possible to derive 3D reconstructions of particle suspensions, colloidal pastes and porous rocks.

4. Diffusion inside the pore network

The understanding of the relationship between the self-diffusion of a fluid embedded in a porous material and the

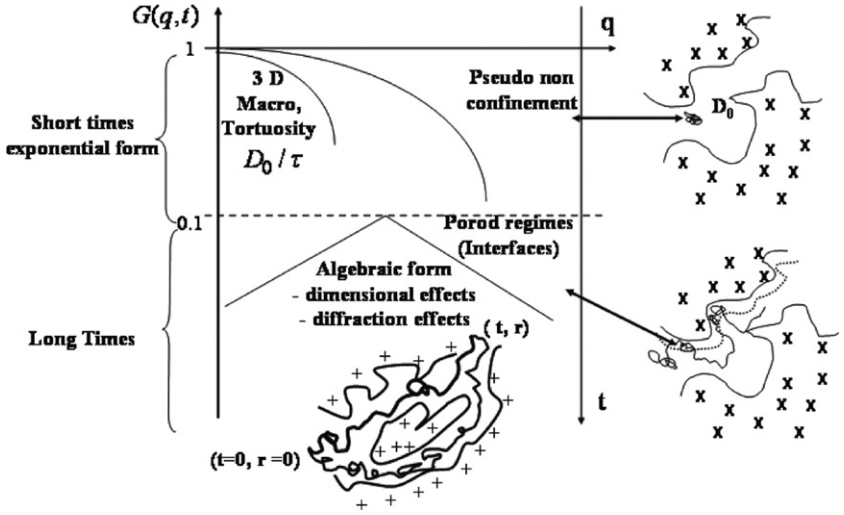

Fig. 9. Road map of the self-diffusion propagator in confinement [36–39].

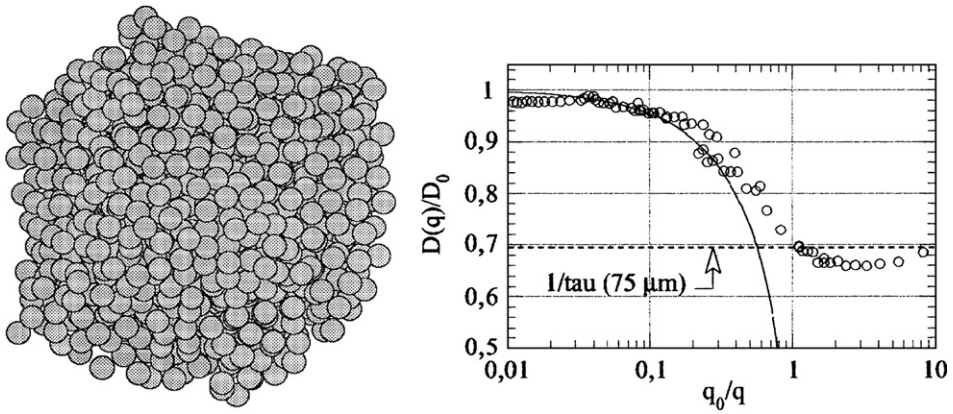

Fig. 10. Relative water diffusion coefficient $D(q)/D_0$ measured in a water-saturated random close packing of monosize glass beads with a diameter $2R=75$ µm. $q_0=\pi/R$ and D_0 is the self-diffusion bulk water. The dotted horizontal line shows the location of $1/\tau$ [36–39].

geometry of the pore network is an active field of research for many scientific communities. During the two last decades, magnetic nuclear resonance techniques have proven to be a powerful tool for studying such processes thanks to the pulsed gradient spin echo technique [33] (NMR-PGSE). This technique gives direct measurements of the 3D Fourier transform, $G(\mathbf{q}, t)$, of the self-diffusion propagator $g_s(\mathbf{r}, t)$. Mitra et al. [34,35] have suggested that in a fluid-saturated material, $G(\mathbf{q}, t)$ may be regarded as a probe of the geometry and the confinement of the pore network. As discussed elsewhere [36–39], it is possible to present a road map of the self-diffusion propagator in confinement. This diagram is shown in Fig. 9. At large q and short time, the probe evolves as a 3D fluid molecule with a bulk self-diffusion coefficient D_0. It does not feel the interfacial confinement. If we increase the time at large q, the probe starts to encounter the interface and it can be predicted and observed [35] the emergence of a dynamical Porod regime running as $\phi S_v/q^4$ where ϕ is the porosity and S_v is the specific surface per unit volume. For small q (large correlation length-scale) and small or intermediate time-scales, we find the usual domain of application of the NMR-PGSE. One probes the diffusive transport at large scales. Generally in the first decade of decay, the propagator $G(\mathbf{q}, t)$ is a Gaussian function of q and an exponential function of t. In the upper left regime, it is possible to get an estimation of the so-called tortuosity factor τ. In the long time limit, the propagator tends to behave as a diffraction pattern of the connected part of the pore network. Sometimes, it may exhibit a correlation peak in the q space (for some model systems) [33]. In this regime, Mitra et al. [34] have proposed an ansatz for the propagator written as:

$$g_s(r,t) = \frac{c\cdot\varphi_p^2(r)}{\Phi^2(4\pi D_\infty t)^{d/2}}\exp\left(-\frac{r^2}{4D_\infty t}\right) \tag{14}$$

with

$$D_\infty = D_0/\tau \tag{15}$$

φ_p^2 r is the isotropic two-point correlation function of the pore space and c is a normalization constant. Eq. (14) exhibits non-Gaussian properties and is sensitive to the dimensionality, d, of the pore network. τ is the so-called "tortuosity", measuring the reduction of diffusion transport in a confined pore network.

4.1. The q-dependent diffusion coefficient [36–39]

In the upper part (exponential time regime) of the road map, we can probe $G(q, t)$ either at constant time or at constant q. The first case is largely discussed in the NMR-PSGE literature and permits one to analyse the time-dependent diffusion coefficient $D(t)$. The second possibility is associated with the q-dependent diffusion coefficient $D(q)$ which is involved in the propagator at fixed q:

$$G(q,t) = \exp(-D(q)\cdot q^2\cdot t) \tag{16}$$

$D(q)$ characterises the self-diffusion at the tunable correlation length-scale $\lambda=2\pi/q$ and gives some relevant information about the transition from microscale to macroscale. We have observed experimentally that Eq. (16) works pretty well in a random close packing of monosize glass beads saturated with water. The mean feature of Fig. 10 is a global decrease of $D(q)$ from the unrestricted value D_0 at low λ to the effective macroscopic value at large λ. However, we clearly observed a minimum located two or three times above the main correlation length ($2R$) of this granular system. These different results can be rationalized in terms of a double porosity model. In fact, the q direction permits to distinguish between an active sub-pore network, globally oriented along the q direction, and a "dead end-like" sub-pore network which plays the role of a slow diffusion regulator. A scaling analysis of this basic scenario permits one to explain the existence and the location of the minimum and also the global shape of $D(q_0/q)$ above $q_0/q=1$.

5. Conclusion

Most porous media exhibit a complex form of disorder. In such case, it is not appropriate to undertake geometric modeling by the iterative association of basic pore shapes such as spheres, cylinders and slits. Thus, disordered media are examples of mesoscopic divided materials and must be characterised in

statistical terms. Several experimental strategies are available to capture and understand the geometrical organisation of porous materials at the mesoscopic length-scale. However, at present it is relatively difficult to use an experimental method to obtain a 3D reconstruction with a spatial resolution well below 0.1 μm. It is possible to adopt an integrated approach by combining available imaging techniques in the real space with the exploration of the q-space, stereology, mathematical morphology and 3D numerical modeling. Two possible strategies are available for 3D modeling. The first is to simulate or to mimic the physical and chemical processes, which control the development of the disordered porous medium and to compare the result with the available experimental geometrical information. Such an approach has to be done on a case-by-case basis but provides an understanding of the physics and the chemistry behind the formation of the porous material. A second strategy is to perform a 3D reconstruction of the material from limited but relatively accurate structural information about the original system, mainly 2D images of a random section and small angle scattering of the matrix. As usual for inverse problems, the question of uniqueness has to be analysed carefully, mainly by including in the 3D reconstruction various experimental, physical and morphological constraints.

In the second part of this paper, we have discussed the relationship between the self-diffusion propagator $g(\mathbf{r}, t)$ of a fluid embedded in a pore material and the geometry of the pore network. The 3D Fourier transform $G(\mathbf{q}, t)$ of $g_s(\mathbf{r}, t)$ permits a multiscale analysis of the confined Brownian motion. We have presented a pseudo-phase diagram (a road map) of $G(q, t)$ in confinement. We discussed the non-trivial properties of a diffusion coefficient $D(q)$ that characterises the self-diffusion at the tunable correlation length-scale $\lambda = 2\pi/q$ and gives some relevant information about the transition from microscale to macroscale.

Acknowledgement

It is a pleasure for me to acknowledge the important contributions of my PhD students and particularly I thank I. Cousin, L. Pothiaud and S. Rodts (with whom, part III was performed). Contribution from and discussions with C. Vigouroux, D. Petit, D.Grebenkov, J-P. Korb and B. Sapoval from PMC, Ecole Polytechnique are also acknowledged.**[PL]**

References

[1] S. Ryde, S. Anderson, K. Larson, Z. Blum, T. Landh, S. Lidin, B.W. Ninham, The Language of Shape: the Role of Curvature in Condensed Matter, Elsevier, 1997, pp. 1–368.
[2] J.S. Beck, J.C. Vartuli, W.J. Roth, M.E. Leonowicz, C.T. Kresge, K.D. Schmitt, C.T. Chu, D.H. Olson, E.W. Sheppard, S.B. McMullen, J.B Higgins, J.B. Schlenker, J. Am. Chem. Soc. 114 (1992) 10834.
[3] B.B. Mandelbrot, The Fractal Geometry of Nature, W.H. Freeman, Sna Francisco, 1982.
[4] M. Sahimi, Flow and Transport in Porous Media and Fractured Rock, VCH, 1995, pp. 1–482.
[5] J.T. Fourkas, P. Levitz, M. Urbakh, K.J. Wahl (Eds.), Dynamics in Small Confining Systems, Materials Research Society, vol. 790, 2003.
[6] F.A. Dullien, Porous Media: Fluid Transport and Pore Structure, Academic Press, New York, 1976.
[7] L.K. Barrett, C.S. Yust, Metallography 3 (1970) 1–33.
[8] J. Serra, Image Analysis and Mathematical Morphology, Academic Press, London, 1982.
[9] I. Cousin, P. Levitz, A. Bruand, Eur. J. Soil Sci. 47 (1996) 439.
[10] L. Holzer, F. Indutnyi, P.H. Gasser, B. Munch, M. Wegmann, J. Microsc. 216 (2004) 84;
L. Holzer, B. Muench, M. Wegmann, P. Gasser, R.J. Flatt, J. Am. Ceram. Soc. 89 (2006) 2577.
[11] L. Pothiaud, P. Porion, E. Lespessailles, C.L. Benhamou, P. Levitz, J. Microsc. 199 (2000) 149–161.
[12] L. Pothuaud, B. Rietbergen, L. Mosekilde, O. Beuf, P. Levitz, C. Benhamou, S. Majumdar, J. Biomech. 35 (2002) 1091.
[13] M. Djabourov, N. Bourret, H. Kaplan, N. Favard, P. Favard, J.P. Lechaire, M. Maillard, J. Phys., II 3 (1993) 611–624.
[14] H. Reiss, J. Phys. Chem. 96 (1992) 4736.
[15] M. Doi, J. Phys. Soc. Jpn. 40 (1976) 567.
[16] S. Torquato, Appl. Mech. Rev. 44 (1991) 37.
[17] P. Debye, H.R. Anderson, H. Brumberger, J. Appl. Phys. 28 (1957) 679.
[18] A. Guinier, G. Fournet, in: John Wiley and son (Ed.), Small Angle Scattering of X-rays, 1955, Chap I.
[19] G. Porod, in: H. Brumberger (Ed.), "Small Angle X-rays Scattering" Syracuse 1965, Gordon and Breach Science Publ., 1967, pp. 1–15.
[20] J. Mering, D. Tchoubar, J. Appl. Crystallogr. 1 (1968) 153–165.
[21] P. Levitz, D. Tchoubar, J. Phys., I 2 (1992) 771.
[22] P. Levitz, in: B. McEnamey, et al., (Eds.), Characterisation of Porous Solid, vol. IV, The Royal Society of Chemistry, 1997, pp. 213–220.
[23] H. Bale, P. Schmidt, Phys. Rev. Lett. 53 (1984) 596–599.
[24] R. Pellenq, S. Rodts, V. Pasquier, A. Delville, P. Levitz, Adsorption 6 (2000) 241–249.
[25] M. Coleman, J. Appl. Probab. 2 (1965) 169.
[26] C. Lin, M.H. Cohen, J. Appl. Phys. 59 (1994) 328–339.
[27] M.Y. Joshi. Ph.D. thesis, Univ. of Kansas (1974).
[28] P.M. Adler, C.G. Jacquin, J.A. Quiblier, Int. J. Multiph. Flow 16 (1990) 691.
[29] P. Levitz, V. Pasquier, I. Cousin, in: B. McEnamey, et al., (Eds.), Characterisation of Porous Solid, vol. IV, The Royal Society of Chemistry, 1997, pp. 133–140.
[30] P. Levitz, Adv. Colloid Interface Sci. 76–77 (1998) 71–106.
[31] P. Levitz, Chap 2 Statistical modeling of pore network, in: K. Sing (Ed.), Handbook of Porous Media, Wiley-VCH, 2002.
[32] M. Rintoul, S. Torquado, J. Colloid Interface Sci. 186 (1997) 467.
[33] P.T. Callaghan, A. Coy, D. Mac Gowan, K.J. Packer, F.O. Zelaya, Diffraction-like effects in NMR diffusion studies of fluid in porous solids, Nature 351 (1991) 467–469.
[34] P. Mitra, P.N. Sen, L.M. Schwartz, P. Le Dousssal, Diffusion propagator as a probe of the structure of porous media, Phys. Rev. Lett. 68 (1992) 3555–3558.
[35] P.N. Sen, M.D. Hurlimann, T.M. de Swiet, Debye–Porod law of diffraction for diffusion in porous media, Phys. Rev., B 51 (1995) 601–604.
[36] S. Rodts, PhD Thesis, Ecole des Ponts et Chaussées, Paris (2001).
[37] S. Rodts, P. Levitz, Time domain analysis: an alternative way to interpret PGSE experiment, Magn. Reson. Imaging 19 (2001) 465–467.
[38] S. Rodts, P. Levitz, Probing confining geometries with molecular diffusion: a revisited analysis of NMR-PGSE experiment, in: J.M. Drake, J. Klafter, P.E. Levitz, R. Overney, M. Urbakh (Eds.), Dynamics in Small Confining Systems V, vol. 651, Material Research Society, 2001, p. T3.6.
[39] P. Levitz, S. Rodts, Recent advances in low dimension and confining materials, Ann. Chim. Sci. Mat. 30 (2005) 345–352.